Double-containment coil with enhanced winding mounting for transcranial magnetic stimulation with reduced acoustic noise

Koponen, Lari M.; Goetz, Stefan M.; Peterchev, Angel V.

DOI:
10.1109/TBME.2020.3048321

Document Version
Peer reviewed version

Citation for published version (Harvard):
Koponen, LM, Goetz, SM & Peterchev, AV 2021, 'Double-containment coil with enhanced winding mounting for transcranial magnetic stimulation with reduced acoustic noise', *IEEE Transactions on Biomedical Engineering*, vol. 68, no. 7, 9311190, pp. 2233-2240. https://doi.org/10.1109/TBME.2020.3048321

HHS Public Access

Author manuscript

IEEE Trans Biomed Eng. Author manuscript; available in PMC 2021 July 01.

Published in final edited form as:

IEEE Trans Biomed Eng. 2021 July ; 68(7): 2233–2240. doi:10.1109/TBME.2020.3048321.

Double-containment coil with enhanced winding mounting for transcranial magnetic stimulation with reduced acoustic noise

Lari M. Koponen,
Department of Psychiatry & Behavioral Sciences, Duke University, Durham, NC, USA.

Stefan M. Goetz [Member, IEEE],
Department of Psychiatry & Behavioral Sciences, Department of Electrical & Computer Engineering, and Department of Neurosurgery, Duke University, Durham, NC, USA.

Angel V. Peterchev* **[Senior Member, IEEE]**
Department of Psychiatry & Behavioral Sciences, Department of Electrical & Computer Engineering, Department of Neurosurgery, and Department of Biomedical Engineering, Duke University, Durham, NC, USA.

Abstract

Objective: This work aims to reduce the acoustic noise level of transcranial magnetic stimulation (TMS) coils. TMS requires high currents (several thousand amperes) to be pulsed through the coil, which generates a loud acoustic impulse whose peak sound pressure level (SPL) can exceed 130 dB(Z). This sound poses a risk to hearing and elicits unwanted neural activation of auditory brain circuits.

Methods: We propose a new double-containment coil with enhanced winding mounting (DCC), which utilizes acoustic impedance mismatch to contain and dissipate the impulsive sound within an air-tight outer casing. The coil winding is potted into a rigid block, which is mounted to the outer casing through the block's acoustic nodes that are subject to minimum vibration during the pulse. The rest of the winding block is isolated from the casing by an air gap, and the sound is absorbed by polyester fiber panels within the casing. The casing thickness under the winding center is minimized to maximize the electric field output.

Results: Compared to commercial figure-of-eight TMS coils, the DCC prototype has 18–41 dB(Z) lower peak SPL at matched stimulation strength, whilst providing 28% higher maximum stimulation strength than equally focal coils.

Conclusion: The DCC design greatly reduces the acoustic noise of TMS while increasing the achievable stimulation strength.

*correspondence angel.peterchev@duke.edu.

DECLARATION OF COMPETING INTEREST

L. M. Koponen, S. M. Goetz, and A. V. Peterchev are inventors on patents and patent applications on TMS technology including the quiet TMS coil technology described in this paper. Related to TMS technology, S. M. Goetz has received research funding from Magstim, and A. V. Peterchev has received research funding, travel support, patent royalties, consulting fees, equipment loans, hardware donations, and/or patent application support from Rogue Research, Tal Medical/Neurex, Magstim, MagVenture, and Neuronetics.

Significance: The acoustic noise reduction from our coil design is comparable to that provided by typical hearing protection devices. This coil design approach can enhance hearing safety and reduce auditory co-activations in the brain and other detrimental effects of TMS sound.

Keywords

Transcranial magnetic stimulation; TMS; coil design; acoustic noise; optimization

I. INTRODUCTION

Transcranial magnetic stimulation (TMS) is a noninvasive method for brain stimulation, with both clinical and research applications. In TMS, an electromagnet coil placed on the subject's scalp is pulsed to create a rapidly changing magnetic field (B-field) which induces an electric field (E-field) in the vicinity of the coil. A typical biphasic TMS pulse lasts only about 300 μs, but must produce peak magnetic field on the order of 1 T, which requires a coil current over 1000 A. The high current and magnetic field produce a mechanical vibration of the coil, which manifests itself in a loud, impulsive sound. The peak sound pressure level (SPL) can exceed 130 dB(Z), and the continuous sound level (SL) during a repetitive TMS (rTMS) pulse train can exceed 110 dB(A), where (Z) refers to flat frequency weighting and (A) designates the most common perceived loudness weighting that emphasizes frequencies between 1 and 6 kHz [1], [2].

The coil sound is a significant limitation of TMS. It poses a risk to hearing [1], [3]–[5] and, with missing or inadequate hearing protection, can cause permanent hearing damage [6]. The loud sound contributes to several adverse side effects of TMS [3], such as headaches [7], [8], and reduces the effective focality since auditory pathways are activated synchronously with the electromagnetic stimulation [9], [10]. During rTMS, the acoustic stimulation further risks unwanted neuromodulation [11], [12].

There are several adopted or proposed approaches to mitigate the effects of the TMS sound. For safety purposes [3], [5], [13], [14], adequate hearing protection during TMS can be obtained with either earmuffs (typical attenuation 20–30 dB for relevant frequencies, i.e., above 1 kHz [15]) or correctly worn earplugs (typical attenuation 20–25 dB for the same frequencies [15]). A consistently good fit of earplugs, though, can be challenging to obtain for all subjects [16]–[19]. Indeed, the reported case of permanent hearing damage from TMS was likely due to incorrectly applied earplugs [6]. Hearing protection devices, even when applied correctly, do not reduce the sound level sufficiently to mitigate the other side effects of the loud sound. Beyond hearing protection, the perceived sound can be reduced with a layer of foam between the coil and the scalp to decrease bone-conduction of the sound [9], [20]. This added distance between the coil and the head, however, reduces both the energy efficiency and attainable stimulation focality—if the coil winding is not optimized for the extra spacing, the efficiency loss is about 10% per mm [21].

In principle, active noise cancellation (ANC) technology could reduce the sound intensity reaching the cochlea. Conventional real-time ANC solutions, however, are typically limited to steady-state sounds and lower frequencies, providing attenuation only for frequencies below 1 kHz, even with in-ear headphones and for sound intensities much lower than TMS

[22], [23]. The TMS coil click has peak SPL that would require extremely powerful headphones, and contains mostly frequencies that are too high for ANC. A TMS-specific offline ANC solution could theoretically solve the problem with high frequencies, but even in simulations, the attenuation for frequencies above 1 kHz was rendered close to zero with a small change in the coil orientation [24]. An ANC solution would also not reduce the bone-conducted sound. Importantly, none of the approaches described so far are sufficient to prevent auditory brain activation. Consequently, noise played through earphones, e.g. fixed 90 dB(A) or individually-leveled white noise, is sometimes used to mask the TMS sound [25], [26]. By practically raising the hearing threshold, such noise masking can reduce unwanted TMS-synchronized auditory activation. However, the loud masking sound itself may disturb noise-sensitive subjects and patients; hinder verbal communication, auditory tasks, or psychotherapy during the TMS session; reduce cognitive performance [27]; and require noise dosimetry to ensure adhering to hearing safety limits [28], [29].

Considering the adverse impact of the loud TMS sound and the limitations of mitigation approaches, it is compelling to develop TMS devices with lower acoustic emissions. This approach is further supported by the conventional hierarchy of hazard controls, in which personal protective equipment is considered the least effective, last-resort solution [30]. Prior to this work, three methods to reduce the sound have been suggested: The sound could be contained by placing the coil inside a medium-to-high vacuum of below 1 Pa [31]. However, such containment would greatly increase the distance between the coil and the head, which would require much more powerful stimulators and pose considerable problems with cooling. Consequently, no such coil has been built. Instead, some commercial MRI-compatible coils use up to 10 mm of acoustic foam to separate the windings from the exterior, which results in a lower sound level, but still at the price of some loss in maximum output and focality [1], [32]. To further reduce the thickness of the sound insulation, our earlier work suggested impeding the sound transmission with multiple layers of different materials: a stiff winding block in a viscoelastic bed, surrounded by an elastic silicone layer and a stiff outer casing [33]. This approach allowed reduced sound while having separation between the winding and the coil surface (4–6 mm) comparable to the upper range for conventional coils (2–5 mm). This coil design was part of our proposed two-pronged approach to “quiet TMS,” involving improved electromechanical coil design and the use of briefer pulses [33], [34].

In this paper, we improve upon the electromechanical coil design for quiet TMS. We present a double-containment coil (DCC) design in which a stiff, electromagnetically-optimized winding block is surrounded by an air cavity—as opposed to solid materials or vacuum—to minimize the sound transmission to the casing. Further, the mounting points of the winding block are designed to have minimal vibrations due to TMS. Finally, the casing has appropriate stiffness and absorption properties, while minimizing the distance between the winding and the subject’s head. We present the DCC design together with computational and experimental measurements of the coil electromagnetic and acoustic output, including a comparison with commercial TMS coils.

II. MATERIALS AND METHODS

A. Coil structure

The proposed coil design is diagramed in Fig. 1. The design has a double-containment structure, in which a potted optimized winding is contained within an independent stiff outer casing, separated from the winding block by a 1.6 mm air gap on the head-facing side and a 17 mm air gap on the other five sides. The purpose of this air gap is to create maximum acoustic impedance mismatch between the stiff winding block, which acts as a sound pressure source, and the stiff outer casing walls. With this construction, most of the sound gets reflected off the interior surface of the outer casing, which delays the sound transmission and increases transmission losses. Consequently, sound pressure inside the outer casing gets amplified, whereas the sound pressure outside the outer casing gets attenuated. To minimize the duration of the sound, two thirds of the air gap on all but the head-facing side were filled with 9 mm thick sound absorbing polyester fiber panels, mounted to the outer casing with a 2 mm air gap for maximum effectiveness.

To minimize the distance to the winding on the head-facing side while retaining structural rigidity, the outer casing (lid) incorporated at its center a shallow circular recession (outer diameter 110 mm, inner diameter 70 mm, depth 4.0 mm) with a thickness of only 2.4 mm (4.0 mm with the air gap). Based on our simulations, such shallow recession does not interfere with placing the coil above any common stimulation location in a representative set of human head models. To minimize the sound transmission via the mounting points for the winding block, their locations were optimized to coincide with nodal points of minimum in-plane vibration of the winding block, determined from an electromechanical simulation. The mounting points were equipped with commercial styrene-butadiene rubber grommets to reduce further this mode of sound transmission via mechanical vibrations.

In the DCC prototype, shown in Fig. 2, the lid was constructed by laminating a piece of 0.8 mm polyurethane foam between a 0.78 mm FR4 sheet and a 4.76 mm FR4 sheet with polyurethane glue (Gorilla Glue Company, USA). The outer casing was built from another 4.76 mm FR4 sheet and 3d-printed sintered walls from nylon 12 (Xometry, USA). These were connected by bolts, and each interface was sealed with a custom laser-cut butyl rubber gasket. The coil winding of the prototype was wound from a rectangular solid magnet wire with height of 4.11 mm, width of 1.45 mm, and heavy-build polyimide-enamel insulation (MWS Wire Industries, USA). An alternative winding implementation using litz wire, which is more efficient for briefer TMS pulses, is described in the Supplementary material. The winding block was constructed by potting the winding with corundum-filled high-strength lamination epoxy (Fibre Glast, USA) (Fig. 2, middle). The potting mold was 3d-printed from nylon 12 (Xometry, USA), and had a minimum wall thickness of 0.7 mm and minimum potting thickness of 1.1 mm (Fig. 2, left). Consequently, the bottom of the coil winding was 1.8 mm above the bottom of the winding block, and the total distance between the center of the coil winding and the coil surface was 7.8 mm, which is comparable with commercial TMS coils [33]. The winding was connected to a commercial TMS device (MagPro R30 incl. MagOption, MagVenture, Denmark) with a 3 m low-inductance TMS-coil cable (Magstim, UK) and a customized orange-type SBE 160 power connector

(Anderson Power Products / Ideal Industries, USA). The cable exit from the outer casing was sealed with an air-tight cord grip, which was separated from the rest of the outer casing with a butyl rubber gasket.

B. Coil winding optimization

The optimization problem for the energy efficiency of TMS coil windings is a convex optimization problem [35]. Such problems have a somewhat shallow energy landscape around the optimum. Thus, minor sacrifices in efficiency can lend substantially improved buildability and desired electrical properties such as higher inductance for a given number of turns with lower coil current requirements. We solved this problem with TMS-coil optimization routines further developed from our prior work [21]. Specifically, we added two new types of constraints: a constraint for the magnitude of coil current density and for the maximum dI/dt for the desired E-field in the cortex. The former is a constraint for a norm, solved similarly to the previous E-field norm constraints [21] and satisfied to a tolerance of 0.001. The updated optimization routines were implemented with MATLAB (Global Optimization Toolkit, Version R2018a, Mathworks, USA).

C. Acoustic simulations

For acoustic simulation of the coil winding block, we built two models. First, a simple 2d model for the in-plane vibrations was used to tune the optimization constraints for the coil winding. Second, a detailed 3d model was created to estimate the required thickness for the winding block. The latter model was further validated post-hoc against the measurements. For the models, the material parameters for the corundum-filled epoxy were estimated with the S-combining rule [36]. Both models were solved with COMSOL Multiphysics (Version 5.3a, COMSOL, USA).

D. Electrical simulations

A TMS coil design has three key electrical parameters: the inductance and resistance of the winding as well as the coupling coefficient to the brain, defined as the ratio between the strength of the E-field induced in the cortex and the rate of change of the coil current. We computed the coupling coefficient for a 85 mm spherical head model [37] with the triangle construction [32], [38] implemented in Mathematica (Version 12.0.0.0, Wolfram Research, USA). The coil inductance and resistance were computed with multipole-accelerated inductance extraction [39] (FastHenry2, Software Bundle 5.2.0, FastFieldSolvers, Italy), and the power cable contribution was modelled with COMSOL.

E. Acoustic and electrical measurements

The acoustic and electrical measurements of the coil were carried out similarly to our previous work characterizing commercial TMS coils [1] with a few minor differences. Notably, we omitted the use of a soundproof chamber and measured the sound in a regular TMS treatment room with the coil facing towards the ceiling, suspended ~ 20 cm above a 15 cm thick open-cell foam panel and all walls at least 2 m from the coil to avoid early reflections. Further, we averaged 9 TMS pulses per condition to suppress the effects of the ambient noise.

Briefly, for acoustic measurements, an omnidirectional flat-frequency-response pressure microphone (M50, Earthworks Audio, USA) was placed 25 cm from the center of the head-facing side of the coil (Fig. 4, inset). The microphone output was fed to a wide-input-signal-range preamplifier (RNP8380, FMR Audio, USA) and then an audio interface with a sample rate of 192 kHz (U-Phoria UMC404HD, Behringer, Germany). The measurement system was calibrated with a 1 kHz, 1 Pa reference sound pressure source (407722, Extech Instruments, USA). We recorded the sound from single TMS pulses at 10% to 100% of maximum stimulator output (MSO) in 10% MSO increments. The continuous sound of rTMS was synthesized from these pulses. To extract the SPL and SL, the audio was processed with the MATLAB Audio Toolbox. We used the electromagnetic artefact removal algorithm as well as low- and high-pass filters described in our previous study [1].

The measurement distance, 25 cm, was chosen to avoid inadequate spatial sampling of the sound in the near field and allow filtering out the electromagnetic artefact from the stimulation [1]. As the sound of TMS attenuates approximately inversely with distance down to about 5 cm [40], we estimated the SPL and SL at the subject's ears, 5 cm from the coil, by adding 14 dB to the measurements at 25 cm [1]. As the DCC is larger than typical TMS coils, we validated this extrapolation approach with laser Doppler vibrometer (LDV) measurements (see Supplementary material).

The induced E-field was measured with a printed-circuit-board-based triangular probe [1] connected to an oscilloscope (DS1052E, Rigol, China) with a sampling rate of 250 MHz. To estimate the effective neural stimulation strength, the recorded waveform was fed into a strength–duration model [41], [42] with a time constant of 200 μs. Additionally, we recorded the maximum rate of change for the coil current from the sensor built into the TMS device. The stimulation strength was calibrated to the average measured resting motor threshold (RMT) of normal subjects extracted from the literature [1].

Finally, to validate our acoustic simulation model and to identify the resonant modes present in our winding block and DCC, we performed non-contact measurement of surface vibrations with an LDV (PSV-400, Polytec, Germany). As both 3d-printed nylon and FR4 scatter the laser, we built small markers from 0.1 mm thick retroreflective vinyl tape. The winding block bottom was sampled with a 5 × 5 grid, and the DCC lid with 41 points on a sparse 13 × 7 grid. In addition, we sampled 4 points from the short and long sides of the winding block and the outer casing (including 1 point on the power connector), and 4 points from the power cable at the coil end with a 5 cm spacing.

III. RESULTS

A. Coil winding and construction

The acoustic simulations of the in-plane vibrations of the winding gave up to four nodal points of greatly reduced mechanical vibrations. The locations of these points depend mostly on the coil size, and to lesser extent on Poisson's ratio of the potting material. For epoxy-like materials (Poisson's ratio about 0.3), four nodal points were identified in the corners of a 180 mm × 130 mm winding block. To move these points away from the corners and place them along the nodal line for the short-edge resonant mode of the winding block, we chose

to implement a slightly larger, 225 mm × 145 mm winding block. To obtain adequate stiffness and sufficiently high resonant frequencies for the out-of-plane vibration modes, the out-of-plane vibration model suggested winding block thickness of at least 40 mm; therefore, we aimed for a thickness of 45 mm. We designed the winding to match the E-field focality of a Magstim 70mm Double Coil in the 85 mm spherical head model. The resulting winding is shown in Fig. 2 (left).

For the potting material, we chose the highest attainable total epoxy-to-corundum mass mixing ratio, 1:3.5 (49.4% corundum by volume). We prepared a small batch with mass mixing ratio of 1:2 (35.6% by volume), which is the highest fill ratio with adequate fluidity to flow around the winding, and a large batch with mixing ratio of 1:4 (52.5% by volume), which corresponds to a self-leveling thick paste. Both batches were de-aired in a vacuum desiccator. The two-stage potting process consisted of covering the winding with the small batch, removing any trapped air under the winding with a vacuum desiccator, and filling the rest of the mold with the large batch. The realized thickness of the potting was 47 mm. To maximize the epoxy strength, the potted winding block was post-cured at 85 °C for three hours.

B. Electrical properties

The simulated coil inductance and resistance were, respectively, 11.1 μH (10.9 μH for the coil winding and 0.15 μH for the power cable) and 19.6 mΩ (14.3 mΩ for the winding and 5.3 mΩ for the cable) at 3.3 kHz. At 1 kHz, the coil resistance dropped to 18.3 mΩ, and at 10 kHz it rose to 25.9 mΩ. These values matched very well the respective measurements of 11.9 μH and 22.2 mΩ at 1 kHz, and 11.8 μH and 33.3 mΩ at 10 kHz, acquired with B&K Precision Model 889A Bench LCR/ESR Meter (B&K Precision Corporation, USA). The unaccounted inductance and resistance likely stem from parasitic inductance and resistance associated with the connections between the winding, coil cable, and measurement probe.

The simulated coupling coefficient to cortex was 1.42 (V/m)/(A/μs) for the entire coil, and 1.67 (V/m)/(A/μs) for the exposed coil winding block. When connected to the MagPro TMS device, the pulse duration for biphasic TMS pulses was 298 μs, which was close to conventional MagVenture coils. The measured coupling coefficients were 1.42 (V/m)/(A/μs) for the coil, and 1.67 (V/m)/(A/μs) for the exposed winding block, matching the simulations. Thus, the outer casing reduced the E-field magnitude and the associated stimulation strength by 15%. Consequently, the stimulation strength at 100% MSO was 275% and 323% of average RMT for the entire coil and the exposed winding block, respectively.

C. Acoustic properties

The SL of the ambient noise in our TMS treatment room was 45 dB(A), and the peak SPL in the 0.2 s measurement window was 71 dB(Z), both about 25 dB above the ambient noise in our earlier measurements inside a soundproof chamber [1]. Given the reduction of SL and SPL for the DCC compared to commercial TMS coils, the ambient noise prevented measuring the sound from subthreshold pulses but was low enough to have negligible effect on the sound recordings near the maximum stimulator output. In addition to the elevated noise background, we further identified a few narrowband ultrasonic sound sources, at 25.0,

45.1, and 51.5 kHz, likely from presence sensors for the room lighting and air conditioning. The strongest of these three sources was at 25.0 kHz and had 1/3-octave sound level of 35 dB. The averaging suppressed these artefacts and had negligible effect (< 0.1 dB) on both SL and SPL at maximum stimulator output, which confirms that it did not reduce the TMS sound.

As the coil sound scales similarly to other air-core TMS coils, we report numbers only for a stimulation strength of 120% RMT for a subject with a top 5 percentile RMT, i.e., about 167% of average RMT [1]. For rTMS, we used the highest repetition rate sustained for several seconds in clinical treatments, 20 Hz [43], [44]. The numbers can be scaled to other stimulation strengths and repetition rates as described in [1].

For the coil winding block, the peak SPL at 167% RMT was 101 dB(Z). With the outer casing, the peak SPL was reduced by 22 dB(Z) to 79 dB(Z) (see Fig. 4). The peak SPL was 18 dB(Z) lower than the quietest coil in our database [1], which is a commercial MRI-compatible coil (MagVenture MRi-B91); 25 dB(Z) lower than the quietest conventional TMS coil; 32 dB(Z) lower than the only coil with a comparable maximum stimulation strength, which has an angled winding topology; and 41 dB(Z) lower than the loudest coil (Fig. 5, top).

The continuous SL of a 20 Hz rTMS train, for the coil winding block, was 78 dB(A). With the outer casing this level was reduced by 15 dB(A) to 63 dB(A). This was 13 dB(A) lower than the commercial MRI-compatible coil, 18 dB(A) lower than the best conventional coil, 22 dB(A) lower than the only coil with comparable maximum stimulation strength, and 32 dB(A) lower than the loudest coil (Fig. 5, bottom).

The 1/24-octave sound spectrums (Fig. 3, second row) indicate that the winding block emits most of its sound in a broad peak around 7 kHz, i.e., at twice the TMS pulse frequency of 3.35 kHz. This is expected for normal TMS coils, as the mechanical vibrations are driven by the Lorentz forces which are proportional to the squared coil current, and hence have their spectral power peak at double the current frequency. The LDV measurement of the winding block bottom showed five resonant peaks that matched their simulated counterparts: 2.2, 4.7, 7.2, 8.8, and 12.0 kHz (Fig. 3, top). For the DCC lid, we observed four resonant peaks: 0.4, 1.1, 2.2, and 4.8 kHz (Fig. 3, bottom). The LDV data further explains the peak at 0.6 kHz, which originates from the vibrations of the coil power connector visible in the middle panel of Fig. 2. The outer casing attenuates frequencies above 4 kHz (Fig. 3, third row), with typical attenuation above 8 kHz of approximately 30 dB. With the outer casing, there is a minimal amount of near-ultrasound content. Thus, the outer casing of the coil acts as an acoustic low-pass filter (Fig. 3, bottom).

IV. DISCUSSION

We presented a new coil design to reduce the sound of TMS. This double-containment coil design maximized the mismatch in acoustic impedance in the path between the winding and the casing [33] without significantly increasing the thickness of the acoustic containment structure. The proposed sound containment provides superior acoustic insulation compared

to a layer of acoustic foam that is approximately twice as thick in commercial MRI-compatible TMS coils, which are relatively quiet but have reduced maximum stimulation strength. Our coil prototype further utilized a winding that was optimized for maximal energy efficiency despite the additional thickness of the casing. This resulted in a coil that, with the same TMS device, has both higher maximum stimulation strength and lower acoustic emissions than any conventional flat figure-8 coil we tested.

As with our previous work [1], we measured the sound levels at 25 cm and extrapolated sound levels to 5 cm to match the typical distance to the subject's ears. The extrapolated values are approximate, as they approximated the coil as a point source and were computed simply by multiplying the measured sound waveform by 5, which scales up the spectrum at all frequencies by 14 dB. Since the coil is not a point source but a distributed sound pressure source, the extrapolation may overestimate some components especially in the high frequencies (beyond 10 kHz). Further, as the low frequencies have wavelength comparable to the measurement distance, the extrapolation may underestimate some components at low frequencies (up to about 3 kHz). As this extrapolation assumes a point source, it can be less accurate for some larger coils. Based on our supplementary LDV data, for the DCC and its winding block in particular, the extrapolation is reasonably accurate for distances down to about 3 cm.

Some aspects of the DCC prototype were designed based on qualitative considerations and approximations for the coil design necessary for our quiet TMS framework, which aims to use high-amplitude ultra-brief pulses [34]. Consequently, the design was optimized to accommodate windings made of litz wire with higher voltage insulation (see DCC* version of the coil described in the Supplementary material). Moreover, since the pulse amplitude required for stimulation with ultra-brief pulses is presently uncertain, the coil design aimed for a high maximum E-field output instead of matching the output to conventional coils, which would let us minimize the sound further. For example, to maximize the coil stimulation efficiency, we chose to implement a moderately thin combination of air gap and lid (4.0 mm). Should this high output not be needed, the sound attenuation by the outer casing can be improved by increasing either the width of the air gap (which reduces the duration of the sound reverberation inside the outer containment) or the thickness of the window in the lid (which further reduces the sound transmission). Alternatively, for the implementation with rectangular solid magnet wire, the coil winding can be redesigned to use a taller, and thus heavier, wire. This will increase the density and stiffness of the winding block, and thus reduce the emitted sound. The optimum values for the three variables depend on both the lid and wire materials and the desired maximum stimulation strength.

V. CONCLUSION

The proposed DCC coil design substantially reduces the instantaneous peak sound pressure level and the continuous sound level during TMS, while providing higher maximum stimulation strength. This can mitigate problems associated with the TMS coil sound.

Supplementary Material

Refer to Web version on PubMed Central for supplementary material.

ACKNOWLEDGMENT

The authors thank Dr. Donald B. Bliss, Dr. David Raudales, and Dr. Mauricio Villa for the discussion on acoustic design; Dr. Brian P. Mann for loaning the LDV; Dr. Jeffrey L. Krolik and Ms. Jessica Centers for enabling the LDV measurement; Dr. Luis J. Gomez for head model data for optimizing the coil casing design; and Ms. Rena Hamdan for help with procurement.

Research reported in this publication was supported by the National Institute of Mental Health of the National Institutes of Health under Award Number R01MH111865 as well as by hardware donations from Magstim. The content is solely the responsibility of the authors and does not necessarily represent the official views of the National Institutes of Health.

REFERENCES

[1]. Koponen LM et al., “Sound comparison of seven TMS coils at matched stimulation strength,” Brain Stimulat., vol. 13, no. 3, pp. 873–880, 5 2020, doi: 10.1016/j.brs.2020.03.004.

[2]. ANSI/ASA S1.4-2014/Part 1. American National Standard Electroacoustics – Sound Level Meters – Part 1: Specifications (a nationally adopted international standard). Melville, NY: Acoustical Society of America, 2014.

[3]. Rossi S et al., “Safety, ethical considerations, and application guidelines for the use of transcranial magnetic stimulation in clinical practice and research,” Clin. Neurophysiol, vol. 120, no. 12, pp. 2008–2039, 12. 2009, doi: 10.1016/j.clinph.2009.08.016. [PubMed: 19833552]

[4]. Goetz SM et al., “Impulse noise of transcranial magnetic stimulation: measurement, safety, and auditory neuromodulation,” Brain Stimulat., vol. 8, no. 1, pp. 161–163, 1. 2015, doi: 10.1016/j.brs.2014.10.010.

[5]. Folmer RL and Theodoroff SM, “Hearing protective devices should be used by recipients of repetitive transcranial magnetic stimulation,” J. Clin. Neurophysiol, vol. 34, no. 6, p. 552, 11. 2017, doi: 10.1097/WNP.0000000000000413. [PubMed: 28914657]

[6]. Zangen A et al., “Transcranial magnetic stimulation of deep brain regions: evidence for efficacy of the H-coil,” Clin. Neurophysiol, vol. 116, no. 4, pp. 775–779, 4. 2005, doi: 10.1016/j.clinph.2004.11.008. [PubMed: 15792886]

[7]. Martin PR et al., “Noise as a trigger for headaches: relationship between exposure and sensitivity,” Headache J. Head Face Pain, vol. 46, no. 6, pp. 962–972, 5 2006, doi: 10.1111/j.1526-4610.2006.00468.x.

[8]. Wöber C et al., “Trigger factors of migraine and tension-type headache: experience and knowledge of the patients,” J. Headache Pain, vol. 7, no. 4, pp. 188–195, 9. 2006, doi: 10.1007/s10194-006-0305-3. [PubMed: 16897622]

[9]. Nikouline V et al., “The role of the coil click in TMS assessed with simultaneous EEG,” Clin. Neurophysiol, vol. 110, no. 8, pp. 1325–1328, 8. 1999, doi: 10.1016/S1388-2457(99)00070-X. [PubMed: 10454266]

[10]. Bestmann S et al., “BOLD MRI responses to repetitive TMS over human dorsal premotor cortex,” NeuroImage, vol. 28, no. 1, pp. 22–29, 10. 2005, doi: 10.1016/j.neuroimage.2005.05.027. [PubMed: 16002305]

[11]. Clapp WC et al., “Induction of LTP in the human auditory cortex by sensory stimulation,” Eur. J. Neurosci, vol. 22, no. 5, pp. 1135–1140, 9. 2005, doi: 10.1111/j.1460-9568.2005.04293.x. [PubMed: 16176355]

[12]. Zaehle T et al., “Induction of LTP-like changes in human auditory cortex by rapid auditory stimulation: an fMRI study,” Restor. Neurol. Neurosci, vol. 25, no. 3/4, pp. 251–259, 5 2007. [PubMed: 17943003]

[13]. Schraven SP et al., “Hearing safety of long-term treatment with theta burst stimulation,” Brain Stimulate., vol. 6, no. 4, pp. 563–568, 7. 2013, doi: 10.1016/j.brs.2012.10.005.

[14]. Kukke SN et al., “Hearing safety from single- and double-pulse transcranial magnetic stimulation in children and young adults,” J. Clin. Neurophysiol, vol. 34, no. 4, pp. 340–347, 7. 2017, doi: 10.1097/WNP.0000000000000372. [PubMed: 28644204]

[15]. Berger EH, “Methods of measuring the attenuation of hearing protection devices,” J. Acoust. Soc. Am, vol. 79, no. 6, pp. 1655–1687, 6. 1986, doi: 10.1121/1.393228. [PubMed: 3522700]

[16]. Toivonen M et al., “Noise attenuation and proper insertion of earplugs into ear canals,” Ann. Occup. Hyg, vol. 46, no. 6, pp. 527–530, 7. 2002, doi: 10.1093/annhyg/mef065. [PubMed: 12176767]

[17]. Neitzel R et al., “Variability of real-world hearing protector attenuation measurements,” Ann. Occup. Hyg, vol. 50, no. 7, pp. 679–691, 10. 2006, doi: 10.1093/annhyg/mel025. [PubMed: 16782739]

[18]. Smith AM, “Real-world attenuation of foam earplugs,” Aviat. Space Environ. Med, vol. 81, no. 7, pp. 696–697, 7. 2010, doi: 10.3357/ASEM.2817.2010. [PubMed: 20597252]

[19]. Nélisse H et al., “Measurement of hearing protection devices performance in the workplace during full-shift working operations,” Ann. Occup. Hyg, vol. 56, no. 2, pp. 221–232, 3. 2012, doi: 10.1093/annhyg/mer087. [PubMed: 22009918]

[20]. Massimini M et al., “Breakdown of cortical effective connectivity during sleep,” Science, vol. 309, no. 5744, Art. no. 5744, 9. 2005, doi: 10.1126/science.1117256.

[21]. Koponen LM et al., “Coil optimisation for transcranial magnetic stimulation in realistic head geometry,” Brain Stimulat., vol. 10, no. 4, pp. 795–805, 7. 2017, doi: 10.1016/j.brs.2017.04.001.

[22]. Vu H-S and Chen K-H, “A low-power broad-bandwidth noise cancellation VLSI circuit design for in-ear headphones,” IEEE Trans. Very Large Scale Integr. VLSI Syst, vol. 24, no. 6, pp. 2013–2025, 6. 2016, doi: 10.1109/TVLSI.2015.2480425.

[23]. Vu H-S and Chen K-H, “Corrections to ‘A low-power broad-bandwidth noise cancellation VLSI circuit design for in-ear headphones’ [2015 DOI: 10.1109/TVLSI.2015.2480425],” IEEE Trans. Very Large Scale Integr. VLSI Syst, vol. 24, no. 6, pp. 2412–2412, 6. 2016, doi: 10.1109/TVLSI.2016.2544342.

[24]. Liu C et al., “Noise analysis and active noise control strategy of transcranial magnetic stimulation device,” AIP Adv., vol. 9, no. 8, p. 085010, 8. 2019, doi: 10.1063/1.5115522.

[25]. Paus T et al., “Synchronization of neuronal activity in the human primary motor cortex by transcranial magnetic stimulation: an EEG study,” J. Neurophysiol, vol. 86, no. 4, pp. 1983–1990, 10. 2001, doi: 10.1152/jn.2001.86.4.1983. [PubMed: 11600655]

[26]. ter Braack EM et al., “Masking the auditory evoked potential in TMS-EEG: a comparison of various methods,” Brain Topogr., vol. 28, no. 3, pp. 520–528, 5 2015, doi: 10.1007/s10548-013-0312-z. [PubMed: 23996091]

[27]. Schlittmeier SJ et al., “The impact of road traffic noise on cognitive performance in attention-based tasks depends on noise level even within moderate-level ranges,” Noise Health, vol. 17, no. 76, pp. 148–157, 4. 2015, doi: 10.4103/1463-1741.155845. [PubMed: 25913554]

[28]. American Conference of Governmental Industrial Hygienists, Threshold Limit Values and Biological Exposure Indices. Cincinnati, OH: ACGIH, 2012.

[29]. MIL-STD-1474E. Department of Defense design criteria standard noise limits. Washington, DC: AMSC 9542, 2015.

[30]. Recommended Practices for Safety and Health Programs. Washington, DC, USA: Occupational Safety and Health Administration, 2016.

[31]. Ilmoniemi R et al., “Stimulator head and method for attenuating the sound emitted by a stimulator coil,” US6503187B1, 1. 07, 2003.

[32]. Nieminen JO et al., “Experimental characterization of the electric field distribution induced by TMS devices,” Brain Stimulat., vol. 8, no. 3, pp. 582–589, 5 2015, doi: 10.1016/j.brs.2015.01.004.

[33]. Goetz SM et al., “Transcranial magnetic stimulation device with reduced acoustic noise,” IEEE Magn. Lett, vol. 5, pp. 1–4, 8. 2014, doi: 10.1109/LMAG.2014.2351776.

[34]. Peterchev AV et al., “Quiet transcranial magnetic stimulation: status and future directions,” in 2015 37th Annual International Conference of the IEEE Engineering in Medicine and Biology Society (EMBC), 8. 2015, pp. 226–229, doi: 10.1109/EMBC.2015.7318341.

[35]. Koponen LM et al., “Minimum-energy coils for transcranial magnetic stimulation: application to focal stimulation,” Brain Stimulat., vol. 8, no. 1, pp. 124–134, 1. 2015, doi: 10.1016/j.brs.2014.10.002.

[36]. McGee S and McGullough RL, “Combining rules for predicting the thermoelastic properties of particulate filled polymers, polymers, polyblends, and foams,” Polym. Compos, vol. 2, no. 4, pp. 149–161, 10. 1981, doi: 10.1002/pc.750020403.

[37]. Deng Z-D et al., “Electric field depth–focality tradeoff in transcranial magnetic stimulation: Simulation comparison of 50 coil designs,” Brain Stimulat., vol. 6, no. 1, pp. 1–13, 1. 2013, doi: 10.1016/j.brs.2012.02.005.

[38]. Ilmoniemi RJ, “The triangle phantom in magnetoencephalography,” J. Jpn. Biomagn. Bioelectromagn. Soc, vol. 22, no. 1, pp. 44–45, 5 2009.

[39]. Kamon M et al., “FASTHENRY: a multipole-accelerated 3-D inductance extraction program,” IEEE Trans. Microw. Theory Tech, vol. 42, no. 9, pp. 1750–1758, 9. 1994, doi: 10.1109/22.310584.

[40]. Starck J et al., “The noise level in magnetic stimulation,” Scand. Audiol, vol. 25, no. 4, pp. 223–226, 1. 1996, doi: 10.3109/01050399609074958. [PubMed: 8975992]

[41]. Barker AT et al., “Magnetic nerve stimulation: the effect of waveform on efficiency, determination of neural membrane time constants and the measurement of stimulator output.,” Electroencephalogr. Clin. Neurophysiol. Suppl, vol. 43, pp. 227–237, 1991. [PubMed: 1773760]

[42]. Peterchev AV et al., “Pulse width dependence of motor threshold and input–output curve characterized with controllable pulse parameter transcranial magnetic stimulation,” Clin. Neurophysiol, vol. 124, no. 7, pp. 1364–1372, 7. 2013, doi: 10.1016/j.clinph.2013.01.011. [PubMed: 23434439]

[43]. Desbeaumes Jodoin V et al., “Safety and efficacy of accelerated repetitive transcranial magnetic stimulation protocol in elderly depressed unipolar and bipolar patients,” Am. J. Geriatr. Psychiatry, vol. 27, no. 5, pp. 548–558, 5 2019, doi: 10.1016/j.jagp.2018.10.019. [PubMed: 30527274]

[44]. Miron J-P et al., “Safety, tolerability and effectiveness of a novel 20 Hz rTMS protocol targeting dorsomedial prefrontal cortex in major depression: an open-label case series,” Brain Stimulat., vol. 12, no. 5, pp. 1319–1321, 9. 2019, doi: 10.1016/j.brs.2019.06.020.

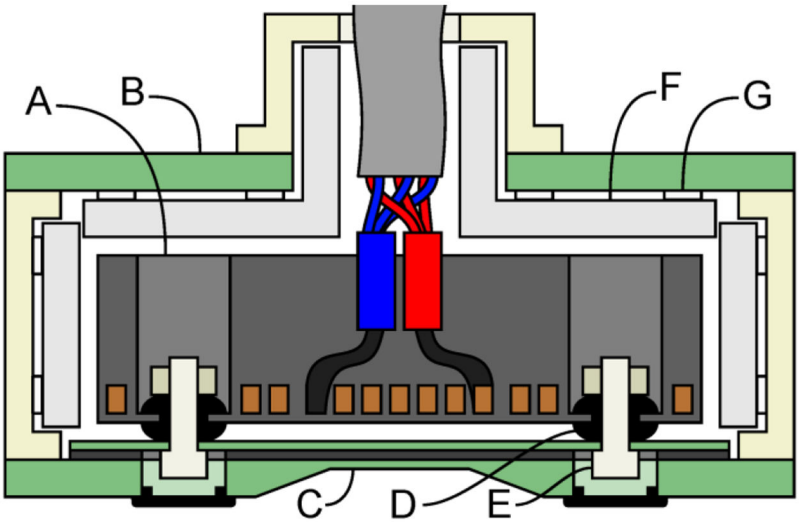

Fig. 1.

The proposed double-containment coil (DCC) comprises a winding block (A), which is essentially a fully-fledged TMS coil, and an outer casing (B) with a lid (bottom) with a central recession to reduce the winding-to-head distance (C). The winding block is mounted flexibly to the outer casing with rubber grommets (D) and nylon bolts (E) at the points of minimal in-plane vibration. To reduce reverberation, the outer casing walls not facing the head are covered with sound absorbing panels (F) mounted with thick foam tape squares (G). Additional views of the coil structure are shown in Fig. 2.

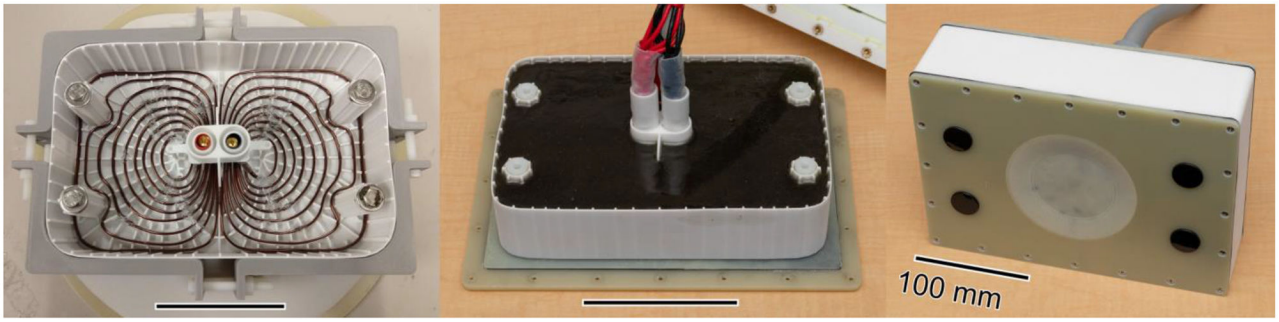

Fig. 2.

The DCC prototype is implemented with an energy-optimized winding made of solid copper wire in a 3d-printed sintered nylon mold (left), potted in place with corundum-filled epoxy (middle), and contained in an outer casing constructed from FR4 sheets and 3d-printed nylon (right). The scale bar in each pane is 100 mm long.

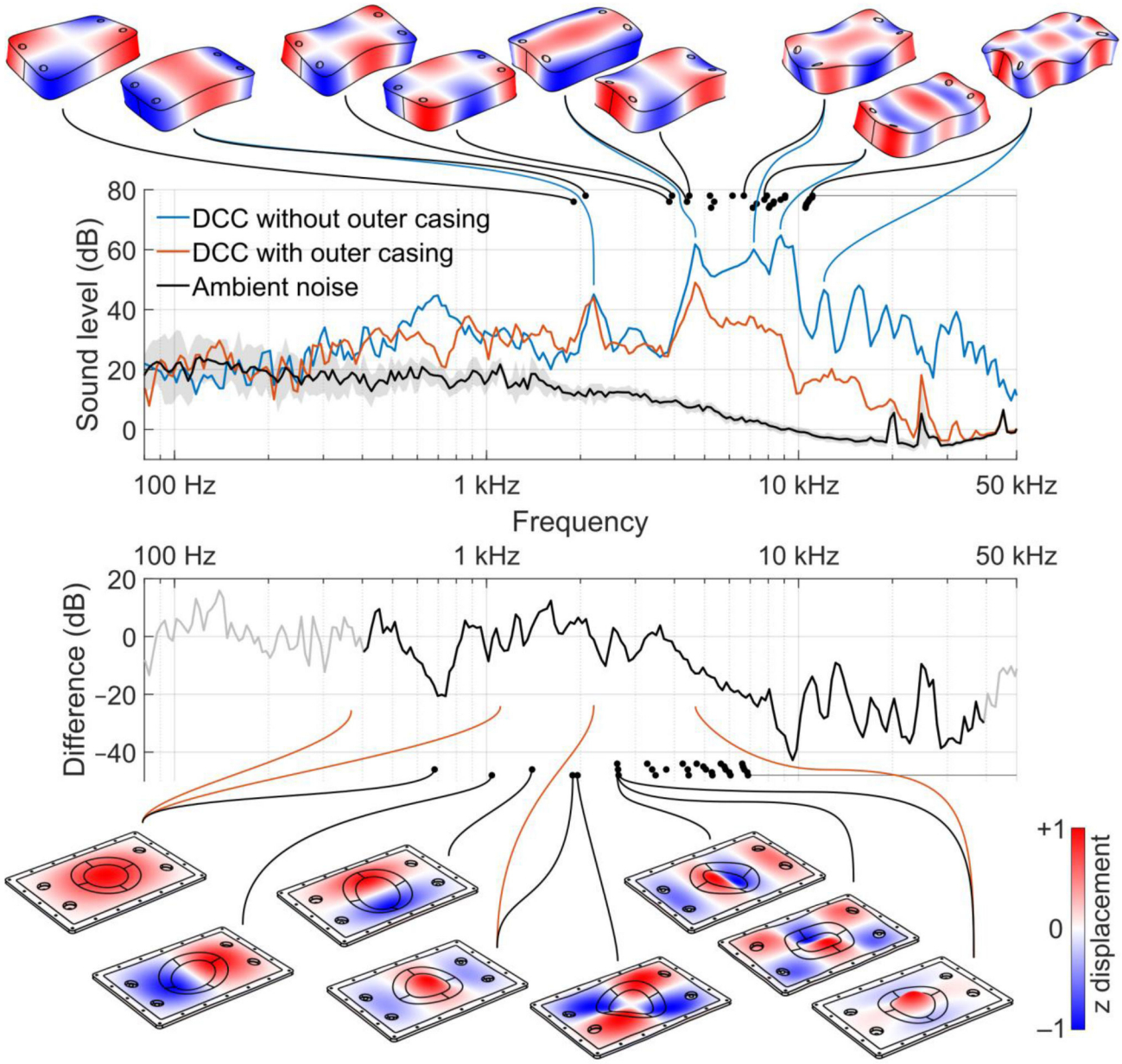

Fig. 3.

Sound spectra and mechanical vibration modes of the prototype DCC. The measured sound spectra plots in dB are compared with the simulated mechanical modes (illustrated with surface displacement plots, black dots denoting the resonant frequencies, and black lines connecting them) as well as the LDV measured modes (linked with blue or red lines). Top: Winding block vibration modes. Second row: 1/24-octave sound level of the winding block and complete coil with outer casing at 167% average resting motor threshold (RMT). To reduce the ambient noise level, 9 pulses were averaged for each trace. The gray band denotes the 95% confidence interval of the averaged ambient noise measurement. Third row: Attenuation provided by the outer casing obtained by subtracting the winding block spectrum from the complete coil spectrum. Despite averaging, the attenuation spectrum at

frequencies below 400 Hz and above 40,000 Hz could not be measured reliably and is therefore grayed out. Bottom: Vibration modes of the outer casing lid. All four LDV measured resonant peaks are likely driven by the winding block motion: the two frequencies at which the lowest mode is active correspond to frequencies at which there is solid motion of the winding block, likely driven by the power cable and coil connector vibration, and the two higher modes are at the exact frequencies of the long and short modes of the winding block, respectively.

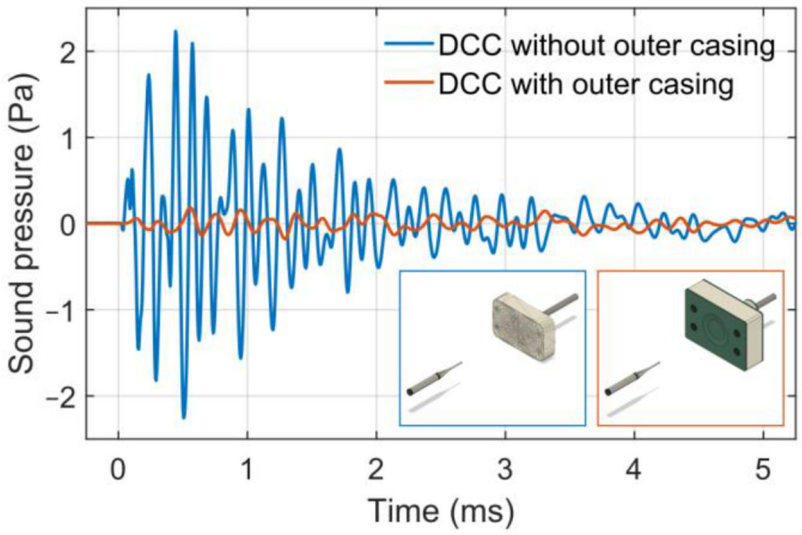

Fig. 4.

Sound pressure waveforms from the DCC prototype and its winding block. In both cases, the microphone was centered 25 cm from the closest head-facing surface (insets). The start of the TMS pulses is at −0.73 ms to compensate for the sound propagation delay in the air. The exposed winding block (101 dB(Z) peak) is compared to the complete coil with outer casing (79 dB(Z) peak). Both configurations are measured for stimulation strength of 167% RMT; thus, the complete coil had 18% higher current to compensate for the thickness of the casing.

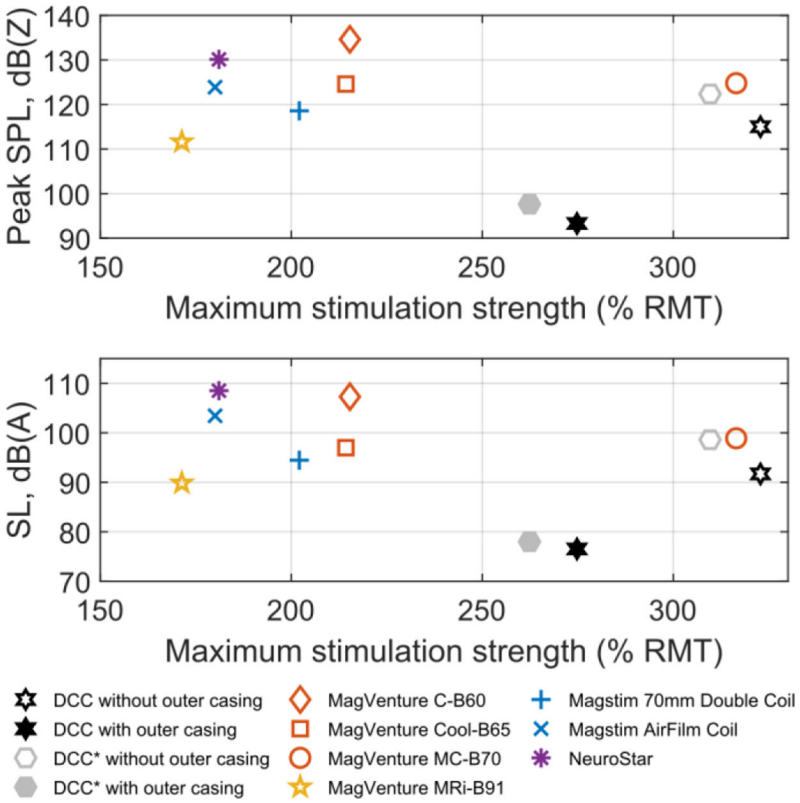

Fig. 5.

Measured TMS coil sound levels as a function of the stimulation strength obtained at maximum stimulator output. The peak SPL (top) and SL of 20 Hz rTMS (bottom) were measured at 25 cm from the coils at 167% average RMT and extrapolated to 5 cm distance by adding 14 dB. Apart from the DCC measurements, the commercial coil data are reproduced from our prior work [1]. DCC* is a litz-wire version of DCC intended primarily for high-voltage ultra-brief TMS pulses; see Supplementary material for more details.